DOI 10.1007/s10946-015-9516-x
Journal of Russian Laser Research, Volume 36, Number 4, July, 2015

CALCULATION OF SELF-GENERATED MAGNETIC FIELDS IN LASER-PRODUCED PLASMAS

Y. B. S. R. Prasad,[1] S. Barnwal,[1] P. A. Naik,[1] P. D. Gupta,[1] E. A. Bolkhovitinov,[2] and A. A. Rupasov[2]*

[1] *Raja Ramanna Centre for Advanced Technology Indore, India*

[2] *Lebedev Physical Institute, Russian Academy of Sciences Leninskii Prospect 53, Moscow 119991, Russia*

*Corresponding author e-mail: rupasov @ sci.lebedev.ru

Abstract

We develop an interactive procedure for estimating the self-generated magnetic fields in laser-produced plasmas using MATLAB software. We use this procedure for analyzing the digital images recorded employing a three-channel polarointerferometer to estimate the self-generated magnetic fields. The three regions of an image recorded using the three-channel polarointerferometer contain all the required information in the form of Faraday rotation (polarimetry), spatial profile of the incident probe beam (shadowgraphy), and electron-plasma density (interferometry). The computer program displays different portions of the image and allows the user to track the interference fringes interactively and displays the calculated spatial profiles of the electron density and the magnetic fields. Using this program, we estimate magnetic fields of the order of 2–4 MG at electron densities $\sim 10^{17}$ cm^{-3} in an aluminum plasma. The program replaces many calculations that have to be done manually.

Keywords: laser plasma, self-generated magnetic fields, Abel inversion, Faraday effect.

1. Introduction

Magnetic fields of the order of few kG to several MG had been detected [1] in laser-produced plasmas. The study of these fields is important as they play a significant role in the inhibition of thermal conduction and in instabilities. Several mechanisms have been reported, including nonparallel thermal sources ($\nabla nx\nabla T$), resonance absorption, and hot electron generation [2, 3], to explain the generation of these magnetic fields. In the case of ultra-intense laser–matter-interaction processes, hot electron generation and inverse Faraday effect [4] are the main sources for the magnetic field generation. In order to understand the laser–plasma-interaction processes better, the location and timing of these magnetic fields are very useful. Initially these fields were detected using techniques like magnetic tapes [5], current probes [6], Zeeman splitting [7], etc.

The estimation of these magnetic fields using Faraday effect was first reported in 1975 by Stamper et al. [1]. In this technique, a plane-polarized light is used for probing the laser-produced plasma in the direction parallel to the target surface. The polarization plane is rotated by an angle proportional to the electron density and the magnetic field along the probing direction. After the Stamper report on Faraday rotation, several different improvised versions of the diagnostics based on Faraday rotation have

Manuscript submitted by the authors in English on July 15, 2015.

been reported in the literature [8]. Using the density information and rotation angle, one can calculate the magnetic fields.

The probe beam used for Faraday rotation measurements is usually generated by splitting a portion of the main laser beam and converting it to higher harmonics (second or third). In all high-power laser systems, the laser beams usually have many small-scale spatial nonuniformities. In addition, the intensity of the probe beam may also change due to processes like scattering, refraction, etc. All these contribute to erroneous estimation of the self-generated magnetic fields as these effects are often neglected. In order to address this issue, simultaneous detection of the spatial profile of the probe is also added to the density and rotation measurements.

We had earlier reported a three-channel polarointerferometer [9,10] that enables simultaneous recording of the Faraday rotation angle (polarimetry), electron density (interferometry), and spatial profile (shadowgraphy) along the same path using a single CCD detector. Magnetic fields of 2–3 MG had been reported in aluminum plasmas using this instrument.

We develop an interactive program SGMF for analyzing the images recorded using this instrument and MATLAB software for obtaining the spatial profiles of the electron density and the magnetic fields produced in the plasma. In this paper, we present the details of this program. The program and other help files can be downloaded from [11].

The next section deals with the Faraday rotation method in general. The description of the three-channel polarointerferometer that we used is given in Sec. 3. Section 4 deals with the procedure for calculating the magnetic fields using our program.

2. Faraday Rotation for Detecting Magnetic Fields

In this diagnostic technique, the rotation of the plane of polarization of a laser beam is measured as it propagates through the plasma. It is based on the principle that the electromagnetic waves with left and right circular polarizations propagating along the magnetic field have different velocities. Therefore, a plane-polarized wave, which can be decomposed into left and right circularly polarized waves with equal intensities, propagating along the magnetic-field direction, remains plane-polarized, but the plane of polarization rotates (Faraday rotation) as it propagates through the plasma. The Faraday rotation angle θ is given by

$$\theta^\circ = 1.5\lambda_p^2 \int \frac{nB_y\, dz}{10^{21}\sqrt{1-n/n_c}}\,, \tag{1}$$

where λ_p is the probe-beam wavelength in μm, z is in μm, n is the plasma electron density in $1/cm^3$, and n_c is the critical density for the probing beam, expressed as

$$n_c = \frac{m\omega^2}{4\pi e^2} = \frac{\pi mc^2}{e^2\lambda^2}\,, \tag{2}$$

and $B_y = B\cos\phi$ is the component of the magnetic field in MG along the direction of the probe-beam propagation (for toroidal magnetic field, ϕ varies from 0 at the top and bottom edges of the plasma to 90° at the level of the axis of the heating beam).

As seen in Eq. (1), the plane of polarization of the probe beam undergoes rotation proportional to the electron density n and the magnetic field component B_y in the direction of the probe-beam propagation. So, in order to calculate the magnetic field, prior knowledge of the electron density is required. Second,

the rotation angle measured is the integrated value along the direction of the probe-beam propagation. The electron density information is obtained by interferometry along the same direction. The space-resolved (radial) profiles of the magnetic field are obtained using the Abel inversion technique assuming cylindrical symmetry.

3. Three-Channel Polarointerferometer

As discussed in the Introduction, in order to accurately estimate the self-generated magnetic fields in laser-produced plasmas, simultaneous recording of a) rotation of the plane of polarization, b) shift in the interference fringes (for electron density measurements), and c) spatial profile of the probe beam (using shadowgraphy) is required. A single instrument (a three-channel polarointerferometer) to do all these three measurements simultaneously was developed at the Laser Plasma Division, RRCAT, Indore in collaboration with the Lebedev Physical Institute, Moscow. In this device, a probe laser beam is split into a number of beams of nearly equal intensities to serve as different diagnostic channels.

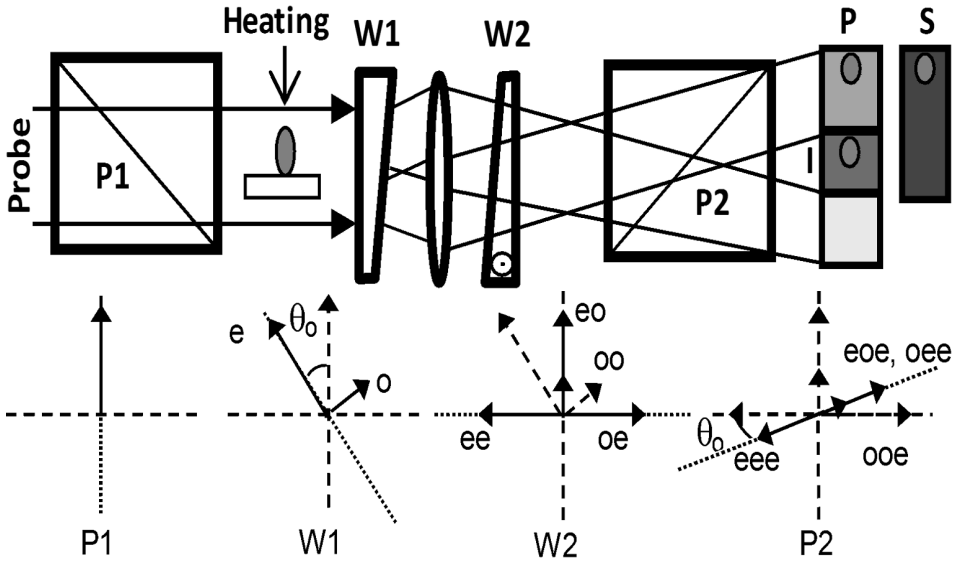

Fig. 1. An optical layout of the three-channel polarointerferometer. Here, the optical axes are shown by dotted curves, input polarizations by dashed curves, and output polarizations by arrows.

To describe the functioning of this instrument briefly (details in [9, 10]), a schematic diagram of the device is shown in Fig. 1. A Glan prism P1 (∼15 mm×15 mm) provides a linearly polarized probe beam that traverses through the plasma under study. Then it passes through a calcite wedge W1 (20 mm diameter) kept at a small angle $\theta_0 (< 5^\circ)$ with respect to the polarizer P1. This splits the beam into two components, extraordinary e and ordinary o.

If I is the intensity of the input probe beam after the polarizer, these two components can be expressed as

$$I_0 = I \sin^2 \theta_0 \qquad \text{and} \qquad I_e = I \cos^2 \theta_0. \tag{3}$$

These components are further split into e and o components by another wedge W2 (20 mm diameter)

kept perpendicular to the polarizer P1. The intensities of these four beams are

$$I_{oe} = I\sin^2\theta_0\cos^2\theta_0 I_{oo} = I\sin^2\theta_0\sin^2\theta_0, \qquad I_{ee} = I\cos^2\theta_0\sin^2\theta_0 I_{eo} = I\cos^2\theta_0\cos^2\theta_0. \tag{4}$$

Of these, the intensity of the I_{oo} beam is small and neglected since the beam crossing angle θ_0 is small. An exit polarizer P2 ($\sim$15 mm$\times$15 mm) is used to equalize the intensities of the other three beams. The intensity components transmitted by the polarizer P2 are expressed as follows:

$$I_{oee} = I\sin^2\theta_0\cos^2\theta_0\cos^2\theta_0, \qquad I_{eee} = I\cos^2\theta_0\sin^2\theta_0\cos^2\theta_0, \qquad I_{eoe} = I\cos^2\theta_0\cos^2\theta_0\sin^2\theta_0. \tag{5}$$

When the polarization plane of the input probe beam is rotated by an angle θ due to magnetic fields in the plasma, the intensities of the above three beams would get modified

$$\begin{aligned} I_{oee} &= I\sin^2(\theta_0 \pm \theta)\cos^2\theta_0\cos^2\theta_0 \qquad \text{for angle of rotation,} \\ I_{eee} &= I\cos^2(\theta_0 \pm \theta)\sin^2\theta_0\cos^2\theta_0 \qquad \text{for density measurement,} \\ I_{eoe} &= I\cos^2(\theta_0 \pm \theta)\cos^2\theta_0\sin^2\theta_0 \qquad \text{for spatial profile of the probe beam.} \end{aligned} \tag{6}$$

One can easily see that only the *oee* component with $\sin^2(\theta_0 \pm \theta)$ factor is sensitive to small changes in the rotation angle, and other components with $\cos^2(\theta_0 \pm \theta)$ factor are not. This image is referred to as the polarogram or the Faraday channel. The spatial intensity profile of this channel is modified only in that region of the plasma where magnetic fields are present. It should be noted here that the reason for introducing a small beam crossing angle θ_0 between different optical components is to know the direction of the magnetic field. In the case $\theta_0 = 0$, the intensity will increase in both cases when the magnetic field is parallel and antiparallel to the probe-beam direction. But when a small beam crossing angle is introduced, the intensity in the Faraday channel will increase only when the magnetic field direction is along the probe-beam direction and will decrease when the magnetic field is in the opposite direction.

The part of the *oee* beam without plasma image is made to overlap with the *eee* beam containing the plasma image, resulting in production of interference fringes. This image gives the interferogram. The wedge angles ($\sim 4^\circ$ and 6° for W1 and W2, respectively) are chosen to obtain fine fringes to provide high spatial resolution, sufficient overlap in the horizontal direction, and well-separated images in the vertical direction. The typical fringe width in our instrument was $\sim$14 μm.

Finally, the *eoe* beam gives the shadowgram, which provides the reference spatial intensity profile of the probe beam for quantitative estimation of the rotation angle from the observed intensity variation in the polarogram. We used a pair of lenses to image the input slit onto the plasma plane, and further imaging of the plasma plane onto a camera for recording the above three images.

In Fig, 2, we present the negative of a typical CCD picture showing the three channels. The bright spots in the polarogram indicate the Faraday rotation of the probe beam. The magnified images of the three channels are shown in Fig. 3 for better visibility.

4. Calculation of the Magnetic Fields

As mentioned earlier, the output of the three-channel polarointerferometer is recorded as a single image on a CCD camera. The image consists of three channels, i.e., polarogram, interferogram, and shadowgram. The image is first displayed on the screen using two MATLAB functions: *imread* and

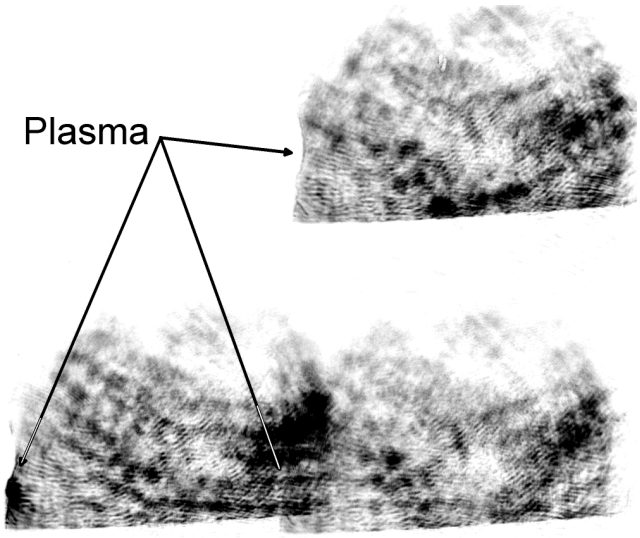

Fig. 2. Negative of CCD picture showing the three simultaneously recorded channels: polarogram (lower right), interferogram (overlapping region of lower images), and shadowgram (top).

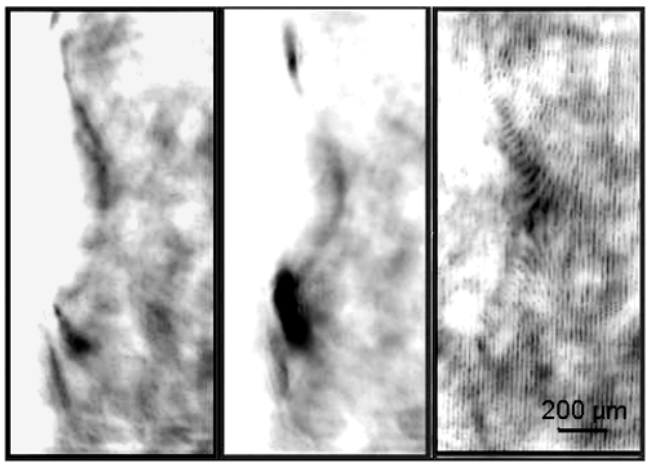

Fig. 3. Expanded view of the three channels: the shadowgram (left), the polarogram (middle), and the interferogram (right).

imshow. In order to estimate the self-generated magnetic fields, the rectangular region, in which the intensity of polarogram is enhanced compared to the other regions, is selected (shown in Fig. 2, in the lower left corner) interactively using *ginput(2)* function. Since the magnetic field is toroidal with azimuthal symmetry, only one side (either the upper half or the lower half) of the image is to analyzed, and we selected the lower half.

Once the region is identified in the polarogram, the corresponding region of the interferogram is displayed (Fig. 4) with a suitable magnification on the screen using the *imcrop*, *imshow* functions with suitable parameters. In order to do this, the offset between the channels must be known in advance. This offset is obtained experimentally by placing a sharp object like a thin cross-wire and then imaging it on the camera. The pixel coordinates of this cross-wire are used for calculating the offset. The accuracy can be improved further by using sharper objects.

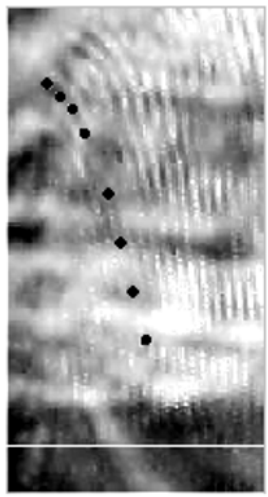

Fig. 4. A magnified view of interference fringes, in which one fringe is tracked.

A fringe is then selected and tracked with the help of a mouse using the *ginput* function. The selection is started from the maximum fringe-shift side and ends, where the fringe shift becomes zero. The selection ends when the Enter key is pressed. (In some versions, this occurs when the *ginput* function receives the same points twice, marking the end of fringe.) After this, all the pixel coordinates on this fringe obtained using *ginput* are available for calculating the fringe shifts and density values between these points. These values are calculated and displayed. The density n is expressed in terms of the fringe shift δ as

$$n = \frac{2\pi mc^2\delta}{\lambda_p e^2 L\Delta x}\,, \tag{7}$$

where m, λ_p, L, and Δx stand for the electron mass, wavelength of the probe beam, dimensions of the

plasma, and fringe width, respectively. Abel inversion (described later) is also carried out to obtain the radial density profile. The calculated density values are fitted using standard methods like cubic spline or polynomial fitting.

Now the intensity data of the polarogram and shadowgram at the points corresponding to this interference fringe (vertical column) are read from the image file, and the angle of rotation is calculated from the ratio I_p/I_s of these intensities. Since $I_P/I_S = \tan^2[(\theta_0 \pm \theta)\cot^2\theta_0]$, one obtains the Faraday rotation angle expressed as

$$\theta = \tan^{-1}(\sqrt{I_P/I_S}\tan\theta_0) \pm \theta_0. \tag{8}$$

It should be noted here that effects like spatial nonuniformities, refraction, scattering, etc. will affect intensities in both (the shadowgram and the polarogram), and by taking the ratio of these intensities, these contributions are taken care of. In the region where the magnetic field is present, the change will be significant only in the polarogram. From this ratio, we calculate the rotation angle. The normalized rotation angle (θ/y) is also calculated and fitted iteratively with spline/curve fitting, and the data are sent for Abel inversion.

4.1. Abel Inversion Technique

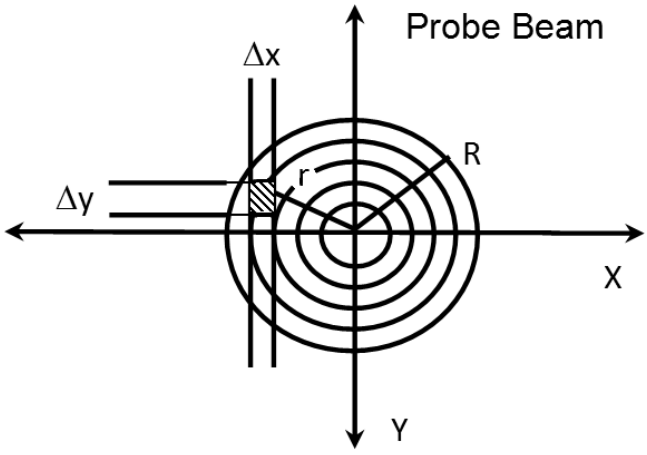

Fig. 5. A schematic of the Abel inversion.

In the case of nonhomogeneous plasmas, the observed fringe shift is the result integrated over many plasma layers having different individual density and thickness values. For plasmas with cylindrical symmetry, the projected density or fringe shifts can be transformed into a radial density distribution using the Abel inversion technique. Here, the radially symmetric plasma is approximated to consist of many concentric cylindrical shells of equal thickness (Fig. 5) within which the density is constant. The Abel inversion transforms the refractive index $\mu(r)$ in terms of the optical path length $D(x)$, which can be written as

$$\mu(r) = -\frac{1}{\pi}\int_0^R \frac{D'(x)\,dx}{\sqrt{(x^2 - r^2)}}\,, \tag{9}$$

where $D'(x) = dD(x)/dx$. The optical path length $D(x)$ can be expressed in terms of the fringe shift, which can be measured from the recorded fringe pattern. This equation can be solved using different methods by expanding the integral equation in terms of linear equations such as

$$\mu(r) = \sum_{i=k}^{N} b_{ik} D(x_k).$$

This calculation has a recursive nature, starting from the outermost cylinder of the plasma $x = R$, where the plasma effect is negligible, and proceeds towards the axis, where the plasma effect is maximum [12]. The coefficients used in this numerical solution are standard ones and are supplied while calculating the plasma densities.

5. Results and Discussion

We performed the experiment for producing the plasma using a high-power Nd:glass laser chain delivering laser pulses of 600 ps – 1.5 ns duration (FWHM). The present experiment was conducted at a laser energy of 5 J in 600 ps. The laser beam was focused on a thick Al slab target to a focal spot of size ∼100 μm (intensity $\sim 5 \cdot 10^{13}$ W/cm^2). The probe beam was obtained by splitting a portion of the main laser beam and converting it into a second-harmonic beam using a KDP crystal. Spatial filters and image relay systems were also used to improve the spatial quality of the probe beam. The probe beam was synchronized with the heating beam using a variable optical delay line. The synchronization was tested with a photodiode. The polarointerferometer was aligned first using a He–Ne laser, and then the probe beam was made collinear with the He–Ne laser beam. The images from the polarointerferometer were recorded using an SLR digital camera (Canon 350D) having a large CCD chip (∼22×15 mm). In order to suppress the self-luminosity from the laser-produced plasma, we used a band pass optical filter for 2ω (0.53 μm) before the camera. To ensure that the probe-beam energy was sufficiently higher than the self-luminosity of the plasma in the 2ω region, another amplifier was used in the probe-beam line before harmonic conversion.

The images recorded in the experiments are shown in Fig. 2. The shift in the selected interference fringe and the calculated electron-density profile are shown in Fig. 6. After an interference fringe is marked using the mouse, the corresponding fringe shifts and electron-density values calculated are displayed as shown in the top row. At this stage, different curve fitting options are used for fitting the electron density. Then the other figures (Fig. 7) give the spatial profile of the rotation angle and the magnetic fields (both measured and fitted). After this, another fringe can be tracked and the corresponding magnetic fields

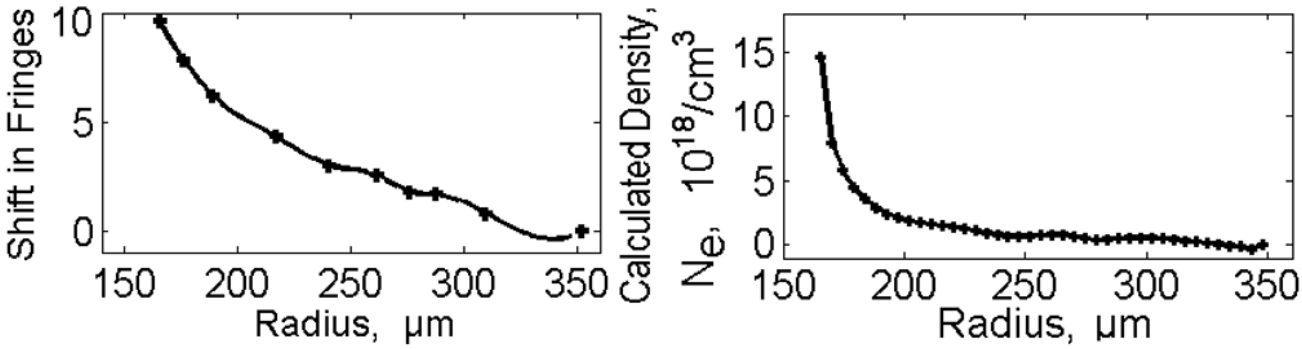

Fig. 6. The fringe shift of a marked fringe and the calculated electron density.

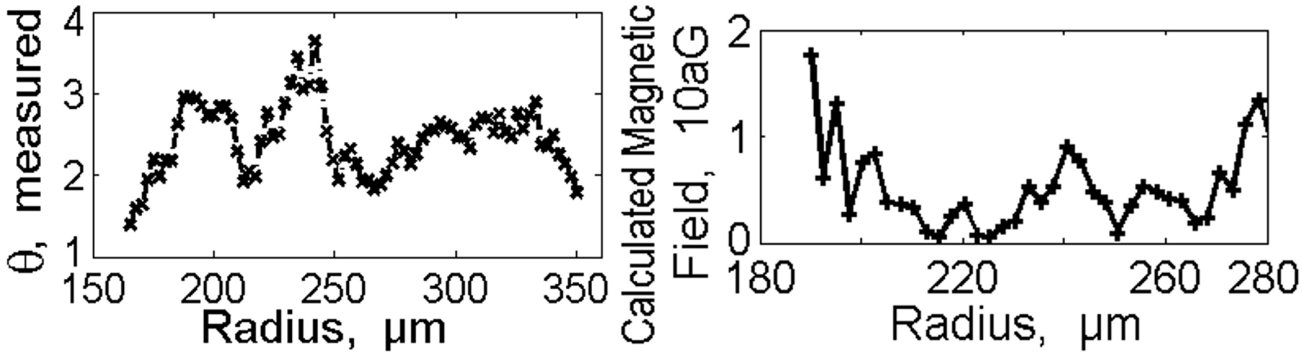

Fig. 7. The experimentally measured Faraday rotation angle and the calculated self-generated magnetic fields.

are calculated. Using several fringes, we can obtain the spatial profile of the magnetic field.

6. Conclusions

We used a MATLAB program to analyze the digital image recorded employing a three-channel polarointerferometer for calculating the self-generated magnetic fields in the laser-produced plasmas. In this program, different regions are chosen interactively. Before this, we were using different methods like Excel data analysis and graphical plotting software to calculate and display the output data. This program simplifies all the calculation and data handling. Different types of fitting can be used for density and magnetic fields. This program can be modified for different needs and experimental conditions. Similarly, the interferogram region can be processed to obtain two-dimensional density distribution, which can be used to get a spatial profile of the magnetic field (2D). These will be attempted in the future.

Acknowledgments

The authors thank the High-Power-Laser team members of the Laser Plasma Division for support during the experiment. Help from the mechanical and workshop team members in fabricating the polarointerferometer is greatly appreciated.

References

1. J. A. Stamper and B. H. Ripin, *Phys. Rev. Lett.*, **34**, 138 (1975).
2. R. J. Mason, *Phys. Rev. Lett.*, **42**, 239 (1979).
3. H. Daido, F. Miki, K. Mima, et al., *Phys. Rev. Lett.*, **56**, 846 (1986).
4. Z. Najmudin, M. Tatarakis, A. Pukhov, et al., *Phys. Rev. Lett.*, **87**, 215004-1 (2001).
5. Y. Sakagami, H. Kawakami, and C. Yamanaka, *Phys. Rev. A*, **21**, 882 (1980).
6. M. G. Drouet and H. Pepin, *Appl. Phys. Lett.*, **28**, 426 (1976).
7. B. B. Pollock, D. H. Froula, P. F. Davis, et al., *Rev. Sci. Instrum.*, **77**, 114703 (2006).
8. T. Pisarczyk, A. A. Rupasov, A. S. Sarkisov, and A. S. Shikanov, *J. Sov. Laser Res.*, **11**, 1 (1990).
9. E. A. Bolkhovitinov, I. A. Krayushkin, A. A. Rupasov, et al., *Instrum. Exp. Tech.*, **50**, 379 (2007).
10. Y. B. S. R. Prasad, S. Barnwal, E. A. Bolkhovitinov, et al., *Rev. Sci. Instrum.*, **82**, 123506 (2011).
11. https://www.researchgate.net/publication/259156605_sgmfprogram
12. W. Lochte-Holtgreven, "Evaluation of plasma parameters," in: W. Lochte–Holtgreven (Ed.), *Plasma Diagnostics*, North Holland, Amsterdam (1968), p. 135.